FINAL REPORT

1. Award number and recipient

DE-FG02-07ER84873
Adelphi Technology, Inc.
2003 E Bayshore Rd
Redwood City, CA 94063

2. Title and principal investigator

Title: Neutron Compound Refractive Prisms
PI: Jay Theodore Cremer

3. Date of report and period covered

Date: June 15, 2011
Period: August 14, 2009 to May 15, 2011

4. Summary of progress, comparison to objectives

The results of the research led to a pulsed electromagnetic periodic magnetic field array (PMF), which coupled with a pair of collimation slits, and a mechanical chopper slit, were able to deflect spin-up neutrons to a band of line-fused neutrons a focal plane heights that correspond to the time-varying magnetic field amplitude. The electromagnetic field PMF produced 5.4 pulses per minute in which each pulse was 50 msec in duration with a full width half maximum (FWHM) of 7.5 msec.

The calculated 7.7 mm vertical height of the band of focused spin-up neutrons corresponded closely to the measured 7.5 mm height of the center line of the imaged band of neutrons. The band of deflected spin-up neutrons was 5 mm in vertical width and the bottom of the band was 5 mm above the surface of the PMF pole. The limited exposure time of 3 hours and the smaller 0.78 T magnetic field allowed focused and near focused neutrons of 1.8 Å to 2.6 Å neutrons, which were in the tails of the McClellan Nuclear Radiation Center Bay 4 Maxwell Boltzmann distribution of neutrons with peak flux at 1.1-1.2 Å. The electromagnetic PMF was expected to produces a 2.0 T peak magnetic field amplitude, which would be operational at a higher duty factor, rather than the as built 7.5 msec FWHM with pulse repetition frequency of 5.4 pulses per minute.

The fabricated pulsed electromagnetic PMF with chopper is expected to perform well on a cold, very cold or ultra cold beam line as a spectrometer or monochromator source of spin-up polarized neutron. In fact there may be a possible use of the PMF to do ultra-cold neutron trapping, see paper by A. I. Frank1, V. G. Nosov, Quantum Effects in a One-Dimensional Magnetic Gravitational Trap for Ultracold Neutrons, JETP Letters, Vol. 79, No. 7, 2004, pp. 313–315. The next step is to find a cold or very cold neutron facility, where further testing or use of the pulsed magnetic field PMF can be pursued.

5. Final Report

1. Fabricate Compound Refractive Prisms with new materials

Under this goal we have considered fabricating material compound refractive prisms (CRPs) from a wide range of materials. As a result of this work, we are concentrating on two materials: Cerroshield as an inexpensive material, especially for relatively higher energy thermal neutrons where longer prisms are required, and Teflon AF for lower energies or where higher performance is required.

We have built and are currently testing material prisms made from Cerroshield, which is a combination of 52.5% Bi, 32% Pb, 15.5% Sn. This metal has an extremely low melting point (95 ºC) and thus is readily molded. We used a previous Al prism as the master for this mold, and produced the prism by pouring the molten Cerroshield over the Al master (Fig. 1a). Due to the low melting temperature of the Cerroshield, a simple hotplate could be used to melt the metal. There was some problem replicating the tips of the prisms, which we believe can be fixed in the future by heating the Al master as well as the Cerroshield. All three components of Cerroshield have good ratios of neutron diffraction to absorption, with Sn and Bi being the dominant effect. The prism was tested as described under goal 3. Sn has a figure of merit about 25% greater than that of Bi, so we have also fabricated a prism by machining square Sn wires tilted on end. We have not yet had an opportunity to test this CRP.

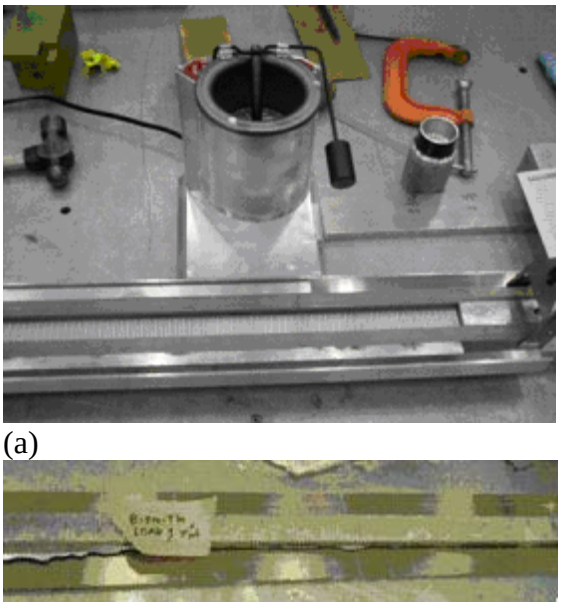

(a)

(b)

Fig. 1. (a) Prism mold and heated crucible for the production of Cerroshield CRPs. (b) The fabricated Cerroshield CRP.

One promising material is Teflon (C_2F_4); however, we have found that for neutron optics, Teflon must be completely amorphous. Teflon AF from DuPont is amorphous, but due to its cost, we wanted to verify that there is indeed no scattering before proceeding with manufacturing a prism, which will cost around $15,000. Fortunately, during the winter, we tested this material as part of another contract to produce neutron lenses, so by simply waiting, we could take advantage of these results for this work. The process of getting the needed absorption measurements and establishing the molding process took longer than expected, but we are now ready to proceed with production. Indeed, we have already made and tested the Teflon AF parabolic lenses and they proved to work as expected. Thus, we are now confident that this material will work for prisms as well (since both optics use the same refractive properties of the material). We describe the calculation and measurement of the absorption length for Teflon AF below. This work was funded under the separate neutron lens contract, but the results apply to CRPs as well. Without this data we would not be confident to proceed with production.

We obtained the Teflon linear attenuation by adding the respective products of the cross section and number density for carbon and fluorine in Teflon. Using a density of 1.78 g/cm3, the calculated absorption constants, μ, are given in Fig. 2. The coherent scattering cross section (5.6

barns for C and 4.0 barns for F at 1.8 Å) dominates the other cross sections (all less than 10 milli-barns). Unfortunately, it is not clear what percentage of the coherent scattering cross section is due to elastic vs. inelastic scattering, which is critical since elastic scattering contributes to refraction but not loss. Also, neutron scattering is highly dependent on local density variations and crystalline structures. Indeed, we chose amorphous Teflon to avoid scattering from microcrystals, but the effect of crystal structure and density variations on the tabulated data is unknown.

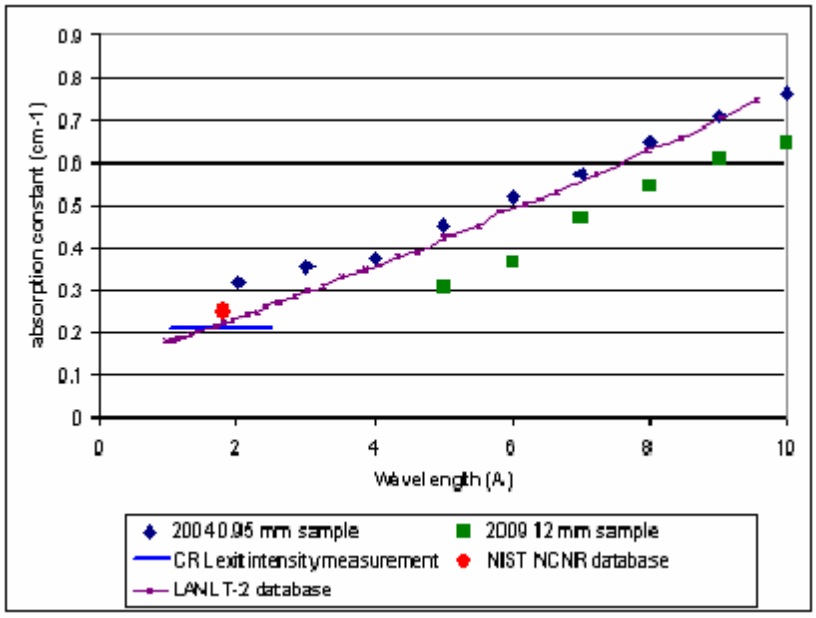

Fig.2. Theoretical and measured absorption coefficients for Teflon.

To get a better understanding of the scattering in amorphous Teflon AF, we made several measurements. At the Low Energy Neutron Source (LENS) at Indiana University, we measured the transmission as a function through our CRL. At LENS, Roger Pynn, our consultant, was able to measure the transmission at wavelengths from 4-14 Å. The facility at LENS was not designed for thermal neutron production and could not measure wavelengths shorter than 4 Å. Prof. Pynn was also able to provide data taken previously with a 0.95 mm thick Teflon sample, though its quality is unknown. Unfortunately, the transmission approached an asymptote at a transmission of 0.97 rather than 1. Prof. Pynn believes that this may have been due to scattering from the front and back surfaces of the material. These effects would not be as significant for the more absorbing 12 mm sample; thus we believe that the 12 mm data is more reliable, but the 0.95 curve can be used to extrapolate the 12 mm data to shorter wavelengths. We also measured the relative absorption vs. radial distance at the exit of parabolic lens made from Teflon AF. This measures the average absorption over the full bandwidth of the Maxwell-Boltzmann spectrum of the beam and is distorted by the bending of rays in the lens, but gives a general indication of the absorption constant. This measurement gives a value of 0.21 cm^{-1}, which corresponds well to an extrapolation from the 12-*mm* sample data. The values from these various measurements and the tabulated value(s) are given in Fig. 2. Based on these measurements, we have decided to use the measured value of 0.21 cm^{-1} for our calculations of future designs.

2. Build Improved Periodic Magnetic Field (PMF) Prisms

Under this goal we have built a more powerful magnetic prism and have initiated the designs of increased power static magnetic prisms with Oersted, Inc. We are continuing with our stated objective of constructing three prisms using the Halbach design. Used in systems from refrigerator magnets to million dollar wigglers for high energy physics, the Halbach configuration uses longitudinally polarized magnets to create a high magnetic field in ferromagnetic spacers. A Halbach wiggler is shown in Fig. 3. The magnetic magnets are placed with their poles facing ferromagnetic spacers. The strength of the magnets on each side of the spacer induces a field in the top edge of the spacer approximately twice that in the permanent magnets themselves. In general, ferromagnetic material can hold much higher magnetic fluxes than that present in permanent magnets, but the ferromagnetic material must be driven externally.

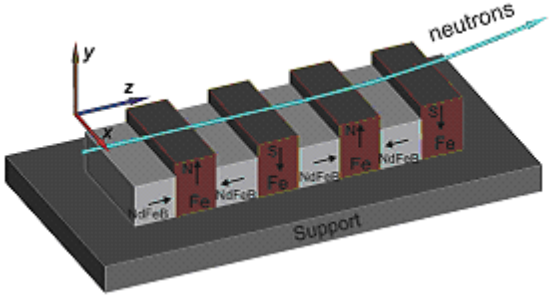

Fig. 3 Shown is the full Halbach Wiggler Configuration. Horizontally polarized permanent magnets force a double strength field in ferromagnetic pole pieces placed between the magnets.

We constructed an inexpensive 3.1 meter long Halbach half-wiggler array that uses 1/2" x 1/2" x 1/8" magnets in a Halbach arrangement and is comprised of 984 NdFeB magnets. Thus, the CRP has 246 half-inch periods. The magnetic field strength at the tip of the pole pieces was measured to be 0.75 Tesla, vs. 0.4 Tesla for the wiggler tested in Phase I. The wiggler CRP is shown in Figs 4 and 5.

3. Demonstrate and test material and permanent periodic magnetic field (PMF) prisms

We tested the material prisms and the magnetic Halbach prism at the McClellan National Radiation Center (MNRC). The measurements were made at MNRC using the experimental setup shown in Fig. 5. Neutrons enter the experimental bay from the reactor core through a small aperture at the lower right in Fig. 5 (this is more readily visible in Fig. 4). The neutron beam is directed upwards at a 22º angle. A pair of Gd slits are used to collimate the beam into an approximately 0.25-*mm* x 3-*cm* beam with a divergence of 0.25 mrad. The beam then travels over the top of the prism, which deflects all (material prism) or the spin-up half (magnetic prism) of the beam upwards. After the prism, the beam travels through a drift space and strikes the Fuji-film neutron sensitive photographic plate used to detect the neutrons. Following exposure, the photographic plate was developed and the resulting image file analyzed to determine the beam intensity profiles. The neutron beam had dimensions approximately 75 *mm* x 1.2 *mm* at the photographic plate. The neutron beam used was much wider than the prism, thus we could determine the undeflected beam position simply by observing the beam outside the prism.

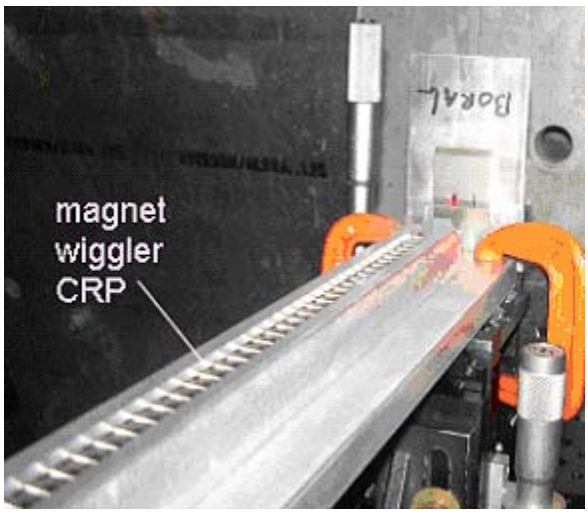

Fig. 4. Picture of the magnetic wiggler CRL in place at the MNRC beam line. The neutron beam enters from the circular aperture at the right, passes through the Gd slits and then over the top of the prism. The individual periods of the compound prism form the ladder-like appearance of the device.

For the magnetic wiggler CRP, since the deflection depends on the beam location above the prism surface, we measured the deflection of the beam for two heights of the neutron beam over the prism. Figure 6 (a) and 6 (b) plots the unperturbed and deflected beams for a neutron beam entering the CRP centered 1.0 *mm* and 0.5 *mm* above its surface. Note that due to the 1-*mm* vertical beam width, part of the deflected beam is clipped by the prism in the second case. We believe that the beam was slightly tilted with respect to the prism surface (about 0.5 milli-radians), which allowed part of the beam passing over the prism to reach the detector when it should have been absorbed by the magnets – some neutrons were at a high enough angle to

Fig. 5. Experimental setup (see text). The CRP is mounted on the long tilted rail. The neutron beam enters from the lower right and after being deflected by the CRP strikes the black imaging plate detector at the upper left.

only strike and transmit through a thin section of magnet.

The observed, deflected beam consists only of the spin-up neutrons, as the spin-down neutrons were deflected into the CRP and did not reach the detector. However, for the 1-*mm* beam center height, some of the spin-down neutrons were deflected downward but did not strike the magnet and reached the detector, which can be seen by the shoulder on the left of the beam profile in Fig. 6 (a). The neutron beam was deflected 1.0 *mm* when it entered closer to the prism and 0.5 *mm* when it was further from the prism. As expected, the beam deflection is stronger closer to the prism surface where the magnetic field is stronger. The beam deflection was about the same as observed from a weaker wiggler in Phase I, but this was due to misalignment of the beam and the prism, so we believe the deflection will improve when we repeat this experiment with more precise control of the neutron beam tilt.

We tested the 30-pole, 15 period permanent magnet PMF fabricated by Oersted Technology with 1.0 cm period and approximately 0.4 T surface magnetic field, shown in the photos in Fig. 7, and the top, middle, and bottom view schematic are shown in Fig. 10. The measured magnetic field is plotted in Fig. 8. At the top of Fig. 9 are plotted for 0.4 T surface magnetic field and 1.0 cm PMF period and initial trajectory heights of 0.5 mm, 0.7 mm, and 0.9 mm, the trajectory height as a function of distance from the PMF entrance for 4.4 Å, 6.0 Å, and 8.0 Å neutrons. The bottom plot of Fig. 9 shows the neutron deflection angle as a function of hypothetical PMF length. In the top and bottom plots of Fig. 9 the initial neutron ray divergence angles at the PMF entrance is assumed zero. The divergence of the neutron beam due to the collimation slits is then added to the plotted neutron beam trajectories of Fig. 9

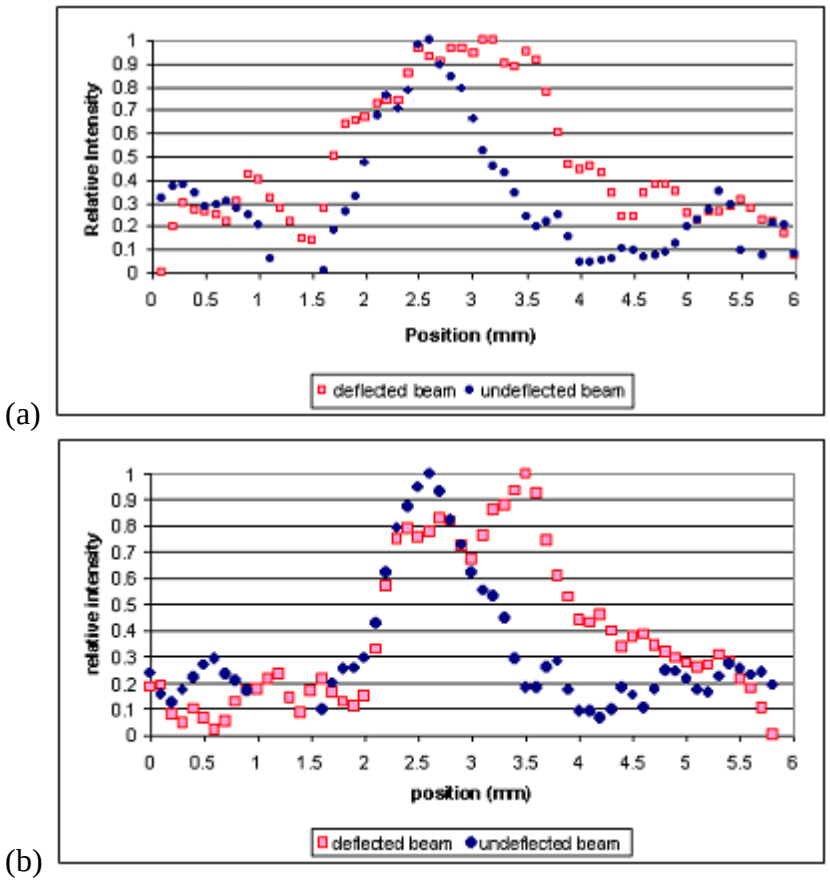

Fig. 6. Plotted are neutron beam intensity profiles of un-deflected beam passing to the side of magnetic CRP and the beam deflected by the CRP. (a) Measurement for a beam center height of approximately 1 mm above the CRP surface. (b) Measurement for a beam center height approximately 0.5 mm above surface.

We fabricated the single pole of a prototype cylindrical magnetic version of the planar PMF, see Fig. 11. A cylindrical PMF

comprised of an axial stack of N annular (washer) magnets, radial magnetized and alternating in polarity, separated by identical aluminum washers, can provide an azimuthally symmetric, periodic radial **B** field throughout its center bore. The cylindrical PMF can thus act as a compound refractive lens to focus the higher energy state, spin-up neutrons and defocus the lower energy, spin-down neutrons in a sufficiently collimated, cylindrical beam with applications as a condenser and/or objective lens in a neutron microscope. The annular magnets are comprised of joined, arc-shaped NdFeB magnets, each arc separately magnetized in the radial direction. The spacer can be designed to encase and bind the mutually repulsive arc magnets, and set the axial spacing between two adjacent annular magnets of opposite radial polarity, which form a period. As an approximation, the planar PMF equations (e.g. focal length) can apply to its cylindrical version with identical number N of periods p, axial magnet Δz_m and spacer Δz_s widths, and bore surface magnetic field amplitude B_0, if the annular magnet inner (bore) radius r_b is equal to the planar PMF critical height, where $r_b = y_f = 0.75\, p/\pi$. An annular magnet, comprised of eight 45 degree sectors, and with

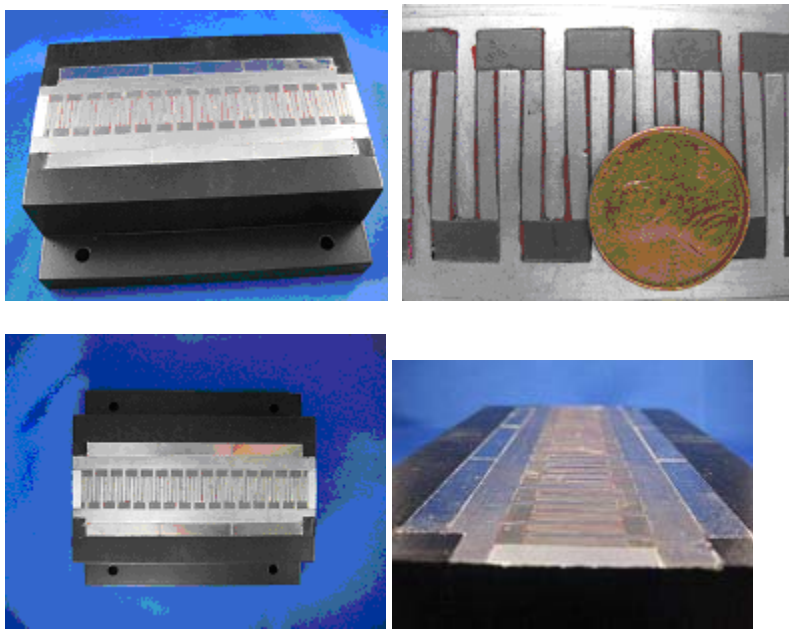

Fig. 7 Photos of 30-pole, 15-period PMF with 1 cm period and 1.0 tesla surface magnetic field

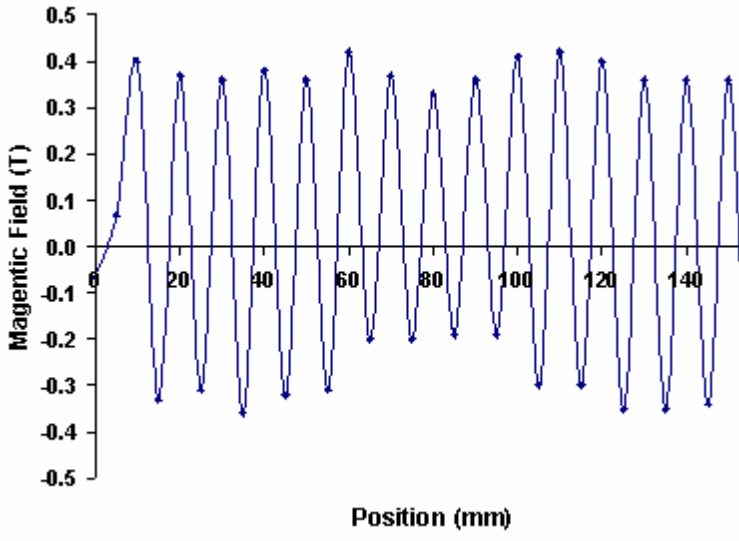

Fig. 8 Measured magnetic field of 30-pole, 15-period PMF with 1.0 cm period, with ~0.4 tesla surface magnetic field

1.59 mm axial width, 1.59 mm inner radius, 12.70 mm outer radius, with about $B_0 = 0.35\ T$ measured on its inner surface, was fabricated for us by J. Stupak of Oersted Technology.

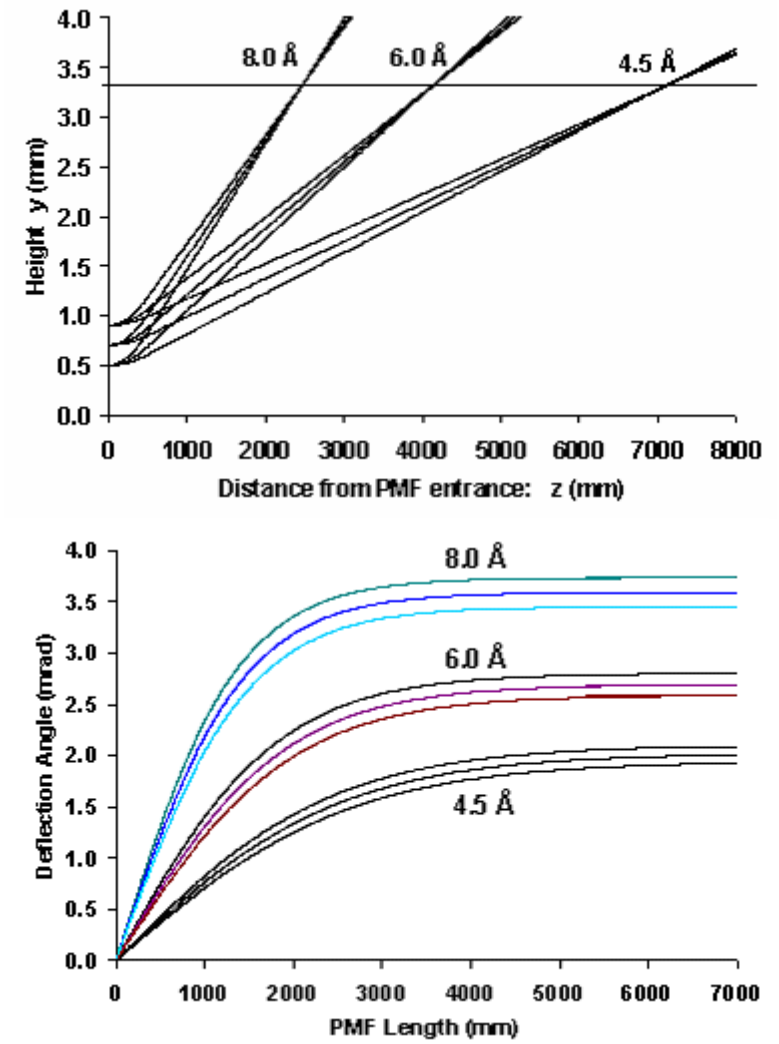

Fig. 9 Calculated for 30-pole, 15-period PMF with 1 cm period and 0.5 T surface magnetic field (top) Neutron trajectory height above PMF plane as function of propagation distance from PMF entrance for 4.5 Å, 6.0 Å, and 8.0 Å neutrons at initial distances of 0.5 mm, 0.7 mm and 0.9 mm above the PMF north-south pole surfaces, and assumed zero initial neutron beam divergence angle. (bottom) Plotted is the calculated deflection angle as a function of a hypothetical PMF length for 4.5 Å, 6.0 Å, and 8.0 Å neutrons, again assuming zero initial neutron beam divergence angle.

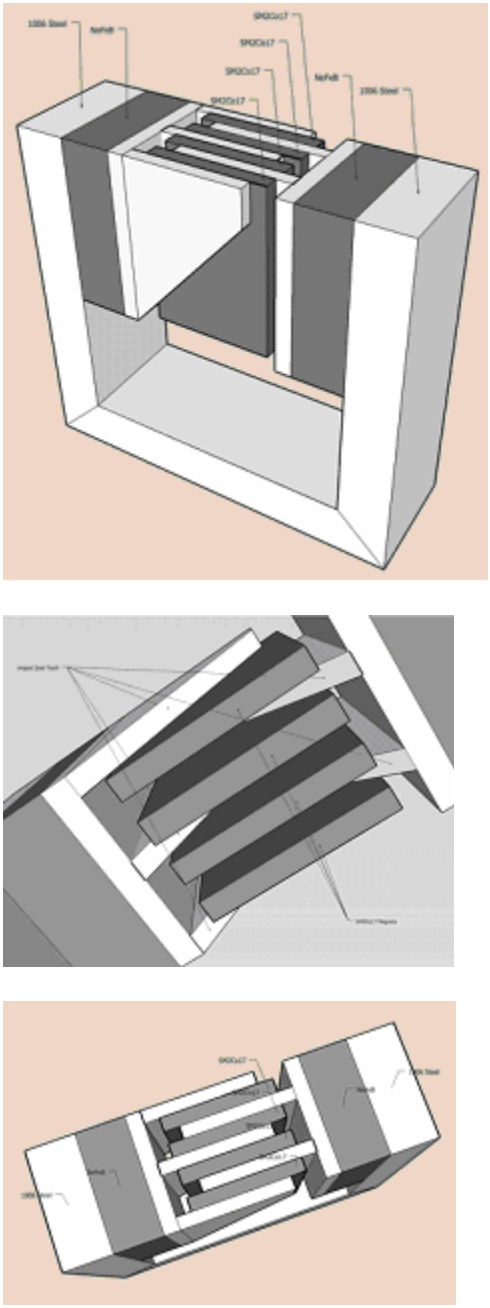

Fig. 10 (top) Shown is schematic of top view of 15-period PMF (middle) Schematic of middle view of schematic (bottom) Schematic of bottom view of PMF.

Fig. 11 Shown is a photo of a two dimensional PMF with alternating N-S-N-S radial magnetic field.

4. Demonstrate and test pulsed Pulse, Electromagnetic Periodic Magnetic Field (PMF)

The PMF was tested at the thermal neutron beam line (Bay 4) at the McClellan Nuclear Radiation Center (MNRC) reactor for its ability to refract, deflect, and separate neutrons vertically by spin state and axially by wavelength. The Bay 4 beam line emerges from an

underground reactor core at a *20 degree* angle relative to the horizontal floor of Bay 4. The Maxwell-Boltzmann distributed thermal neutrons pass from the reactor water core into the Bay 4 beam tube through a graphite (moderator) end plug, and then pass through a *28 cm* long sapphire crystal, which improves the thermal content by reducing the relative number of higher energy neutrons and gammas.

From the sapphire crystal the neutrons emerge from a *3.2 cm* square source aperture in a boron carbide shielding plate, and propagate *3.0 m* through a collimation tube to a horizontal slit, which is mounted on the aluminum face plate of the beam tube. The beam tube has scraper structures along its walls that aid in the removal of divergent neutrons and suppresses neutron scatter. The first horizontal slit, which is set on the aluminum face plate, has horizontal width *9.5 mm* and vertical height *0.5 mm*, and beyond this first slit is a massive sliding concrete door that opens to provide neutron exposure into Bay 4. The flux distribution $\Phi(\lambda)$ of the neutron beam incident at the PMF is a wavelength dependent Maxwell Boltzmann distribution, given by

$$\Phi(\lambda) = \left(\frac{\lambda_p}{\lambda}\right)^5 \exp\left[2.5\left(1-\frac{\lambda_p^2}{\lambda^2}\right)\right] \tag{1}$$

The peak neutron flux $\Phi_p(\lambda)$ occurs at wavelength $\lambda = \lambda_p$, where $\lambda_p = \lambda_t\sqrt{2/5}$, which MNRC estimates to be $\lambda_p = 1.1$ Å.

The first collimation slit is mounted on the aluminum face plate. The first slit is 2 cm wide and 1.0 mm vertical height slit and was aligned with the wall laser. The PMF is mounted on a Thor Labs *2.5 meter* long optical rail, see Fig. 12. The second slit is mounted at the on the Thor Labs rail at the entrance of the PMF at a 1.5 m downstream distance from the first slit. The second slit is also 2 cm wide with a vertical height of *1.0 mm*, which matches the first slit. The rail is tilted at *20 deg* relative to the floor to be aligned parallel with the neutron beam. The two collimation slits are aligned with the PMF via a laser, which is mounted on the downstream beam-stop wall. This wall laser provides a straight line laser beam, parallel to the neutron beam, between the center of the neutron source aperture and the neutron imaging detector. The small, square source aperture with side dimension $D = 31.75$ *mm*, and the long length of flight $L = 10^4 mm$ from the neutron source aperture to detector, produce collimation $L/D = 315$ without the slits, which corresponds to divergence angle $\theta_{div} = D/L$ or $\theta_{div} = 3.2x10^{-3} rad$.

The two collimation slits are needed to reduce the neutron beam's vertical divergence angle to less than the PMF deflection angle. The two slits have an average vertical height of *1.0 mm* and are separated by *1.5 meters*, and thus the two slits reduce the neutron vertical divergence angle by a factor of ten to $\theta_d = 6.7x10^{-4} rad$ at the PMF entrance, where the neutron flux is $1.3x10^6 n/cm^2/s$ for neutron energies below *0.1 eV*. The collimated neutron beam passes through the PMF and drift space to the downstream Fuji-film[17] neutron imaging plate or IP. A diverging ray after the pair of collimation slits has vertical divergence angle $\theta_d = 6.7x10^{-4} rad$ at the PMF ray entrance, and the ray will attain a vertical height of 3.5 mm in the maximum 5.3 meter distance from the PMF entrance to the Fuji film plate imaging plate, which is placed at the Bay 4 beam stop next to the alignment laser.

In Fig. 13 (top) is plotted the calculated trajectories of the 1.8 Å, 2.2 Å, and 2.6 Å neutrons at initial heights 0.01 mm, 0.53 mm, and 1.06 mm above the PMF pole surfaces in which the initial neutron beam divergence is assumed to be zero. In Fig. 13 (bottom) is plotted current pulse amplitude as a function time. The electromagnetic PMF magnetic field is produced by the current pulse through the serpentine windings around the iron rectangular bars, which act as the north and south magnetic poles which form 2 cm periods with a 2 cm transverse pole width and a 1 cm axial pole width. The serpentine winding 21.24 milli-farad capacitance, 0.439

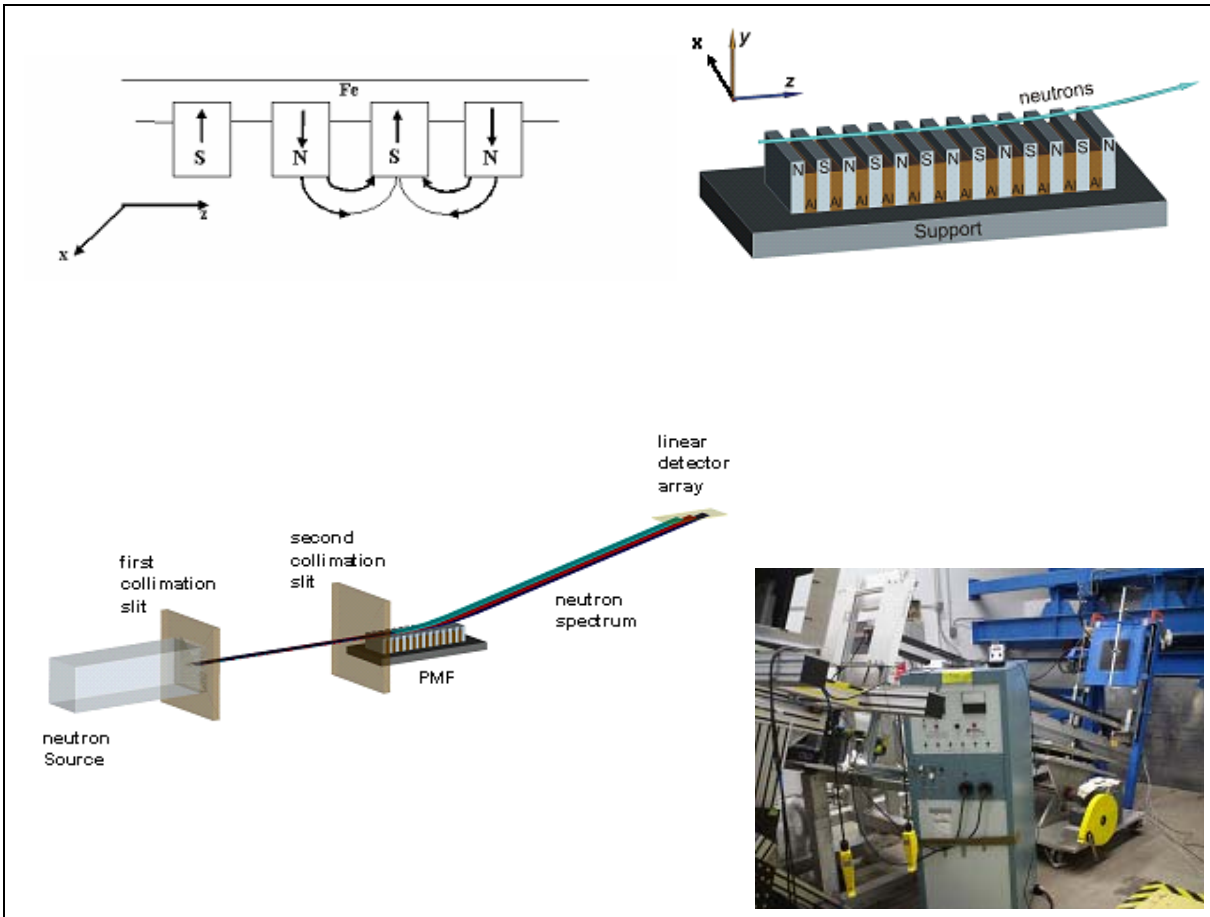

Fig. 12 The electromagnetic PMF provides equal and opposite vertical deflection of neutron spin states and axial separation of neutron wavelengths. The higher energy state, spin-up neutrons ($\mu_{||}$ aligned anti-parallel to B-field direction) are deflected upward from PMF magnet surface. The pair of collimation slits reduces the initial neutron beam divergence to less than the deflection angle acquired by the neutrons in the PMF. The PMF provides 1-D horizontal line-focusing of neutrons along an axial line parallel and above the PMF surface in which the focal distance measured from the PMF exit increases proportionally with neutron energy.

ohm resistance, and 0.2 milli-henry inductance with an applied 700 volts to produce the has a 7.5 msec FWHM current pulse, which could be repeated at 5.4 pulses per minute. The resulting magnetic field pulse was then also 7.5 msec FWHM duration with a repetition frequency of 5.4 pulses per minute. The peak magnetic field at the pole surfaces was estimated to be +/- 0.78 T.

The Fuji-film IP is used to provide alignment and imaging. For initial alignment of the two collimation slits with the PMF, the IP is initially mounted at the end of the PMF. For final

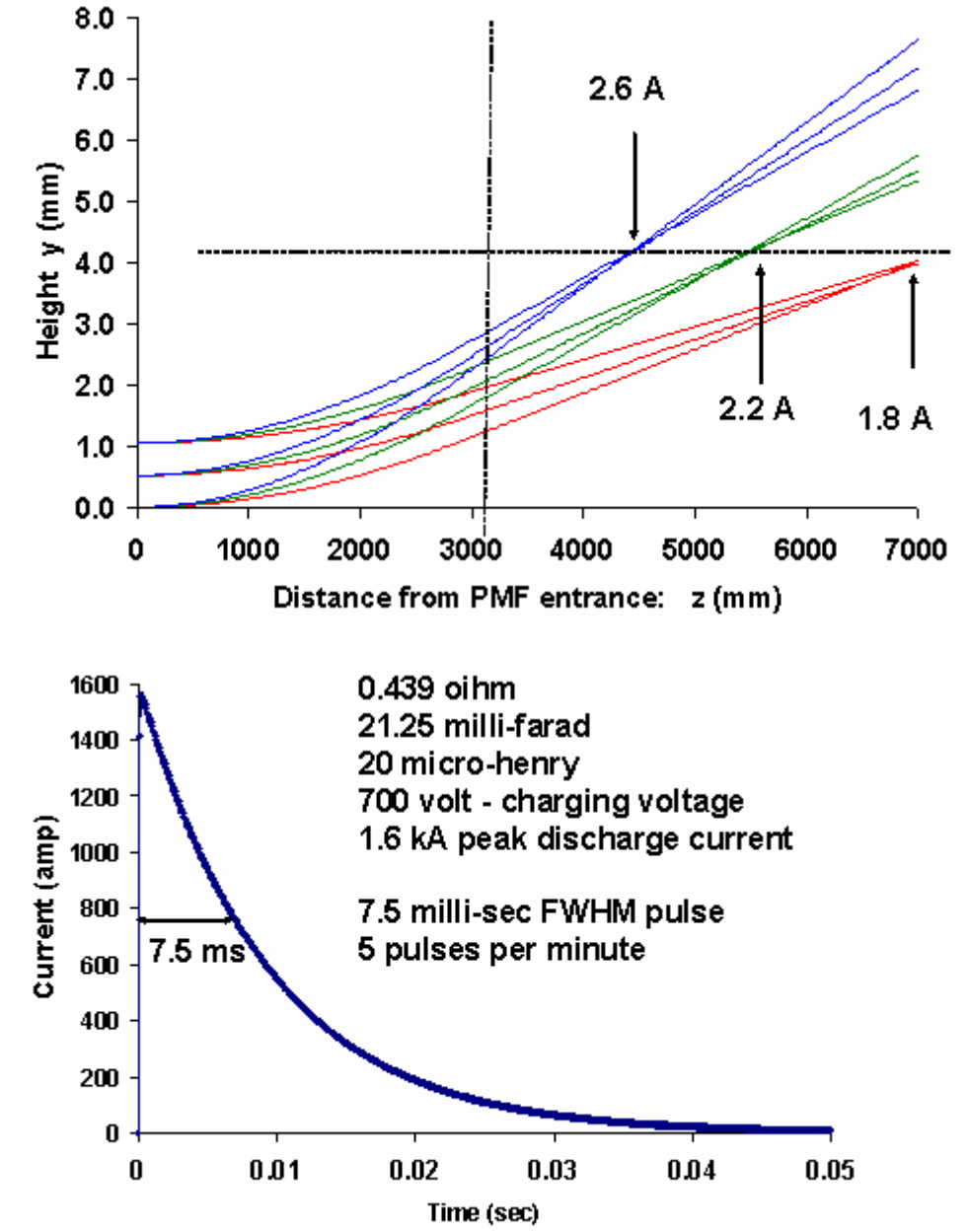

Fig. 13 Calculated for 300-pole, 150-period PMF with 2 cm period and 0.78 T surface magnetic field (top) Neutron trajectory height above PMF plane as function of propagation distance from PMF entrance for 1.8, 2.2, and 2.8 A neutrons (bottom) Plot of the electromagnetic PMF magnetic field pulse, which has a 7.5 msec FWHM and a repetition frequency of 5 pulses per minute.

alignment the IP is set near the beam-stop wall, which is situated at maximum distance *5.64 meters* downstream from the 2nd slit at the PMF entrance. For imaging the IP is mounted on a

precision Bosch movable detector platform that is tilted *20 deg* to match the Bay 4 beam line. The detector can thus be translated toward the PMF, and scan the line-focused, spin-up neutrons whose energy decreases as the detector approaches the PMF. The FCR XG-1NDT Fuji-film neutron imaging system uses an integrating, position sensitive detector (PSD) with high *18.2%* quantum efficiency (DQE), *50-μm* pixels, and 5 orders of dynamic range, and is based on the effect of photo-stimulated luminescence (PSL). One can obtain large area (*23 cm* x *25 cm*) static, single shot images with the Fuji-film IP. The software package, Dynamix Image Share Viewer, was used to display the Fuji-film neutron images.

The Electromagnetic Pulsed System consists of two major components, the pulse generator and periodic magnetic array. The pulse generator is enclosed in a floor-mounted cabinet, and contains a high-voltage power supply, storage capacitors, a solid-state switch, re-circulating high-power diode, and other components. The field is momentary, with pulse lengths which can be varied using variable-capacitor technology. The peak charging voltage is 800 volts. The electromagnetic PMF was 3 meters long with 150 periods with 2 cm periods and a measured peak magnetic field of 0.6 T at insulated surface of the PMF, which was 1.0 mm above the ferromagnetic poles. The surface magnetic field, which could not be measured, was estimated to be 0.78 T. More details of the electromagnetic PMF fabricated at Oersted Technology are given in the Appendix.

The PMF power supply provides a 0-800 Volts output pulse with solid-state switching using SCRs (no mercury-filled vacuum tubes) and ECS(Electronic Capacitance Switching^{TM}) variable capacitance and 36,000 amperes peak magnetizing current with a built-in automatic peak output current meter with output current measurement by integral pulse transformer. The power supply has a BNC jack for current monitoring by oscilloscope, 0-1 V., isolated from high voltage locking safety switch with key, and pulse control electronics for interface to a remote computer, and pulse shutoff verification and pulse series control. The 280 lb PMF power supply is in stand-alone cabinet on locking casters, 22 in. wide x 31 in. deep x 63 in. high (56 cm x 79 cm x 160 cm).

The PMF electromagnet could be pulsed 5.4 times per minute and produced peak magnetic field 0.78 T in a short pulse of 7.5 msec full width half maximum (FWHM) without overheating. The focal plane for the 0.78 T magnetic field is 4.5 mm for all wavelengths. Within the 5.3 meter distance from the PMF entrance to the beam stop and alignment laser, the 0.78 T magnetic field is expected to deflect and focus spin-up neutrons in the focal plane 4.5 mm above the PMF rail surface with wavelengths from 1.8 A to 3.0 A. The highest energy 1.8 Å spin-up neutrons are focused at the beam stop and the lowest energy 3.0 A neutrons are focused at the end of the PMF rail, see Fig. 13. The capacitance could be varied from 1.25 milli-farad to 81.25 milli-farad by switches on the PMF power supply unit. The serpentine winding had a fixed inductance of 0.274 milli-henry and 0.439 ohm resistance. By changing the capacitance at a set maximum voltage of 700 volts, one could vary the full width half maximum (FWHM) pulse length from a few milli-seconds to 27 milli-seconds.

Fig. 14 Photos of measurement of the peak electromagnetic field of the PMF. The Hall probe can record the peak of short magnetic field pulses. The maximum positive and negative polarity magnetic fields measured at the PMF surface was about +/- 6.1 kilogauss. The Hall probe element is 0.5 mm from its outer surface and the insulation on the PMF surface is 1.0 mm, so that the peak surface magnetic field was estimate to be about +/- 8.0 kilogauss.

The short 7.5 msec FWHM magnetic field pulse PMF was measured with an AlphaLab, Inc. DC magnetometer, Model GM2, which has a dynamic range from 0 to +/- 3.0 T (30 kG) with readings in kilogauss (kG), where 10 kG is one tesla (T). The model GM2 is able to record the peak DC magnetic field of pulses as short as 2.0 msec, which was much shorter than the PMF magnetic field pulses. The active Hall probe was 0.5 mm from the probe surface, and the electric insulation on the PMF was about 1.0 mm, which limited surface magnetic field measurements of the PMF at a minimum distance of 1.5 mm. The measured peak +/- 6.1 kG readings with the active Hall probe were inferred to correspond to +/- 7.8 kG at the PMF north and south pole surfaces, assuming exponential decrease of the magnetic field from the PMF pole surface. Photos of the peak magnetic field measurements of the PMF are shown in Fig. 14. Also shown in Fig. 14 is the power supply for the PMF.

The first set of experiments with the PMF without the chopper gave inconclusive results due to the 7.5 msec FWHM magnetic field pulse and the 11 second charge time, which yields a magnetic-field-on duty factor of 0.068% (6.8×10^{-4}) chopper set up is shown in Fig. 15. The continuous neutron and gamma noise strikes the expected focal plane region (4.5 mm above

PMF plane) during the 11 second charging period; thereby masking the small signal line-focus image of the focused spin-up neutrons. The PMF was not able to line focus the 1.1 Å to 1.2 Å peak flux of neutrons of the MNRC Maxwellian distribution within the 5.3 meters maximum focal distance in Bay 4. The lower than expected 0.78 T was only capable of line-focusing the small flux of 1.8 to 3.0 Å spin-up neutrons which lie within the tail of the warm Maxwellian distribution for the MNRC neutrons, which are well above room temperature.

As a result, a chopper was designed, fabricated, and tested. The chopper is a 2 cm wide and 1 mm vertical width slit in neutron-absorbing boral and is set in the normally closed position in which the chopper slit is aligned above the entrance slit at the PMF rail entrance. The chopper slit is placed at the PMF entrance just downstream of the second collimation slit. Only a few centimeters separate the chopper slit from the upstream 2nd collimation slit. The entrance slit at the PMF rail entrance is 2 cm wide and 1 mm in vertical height, which matches both the 1.5 meter upstream slit on the aluminum face plate

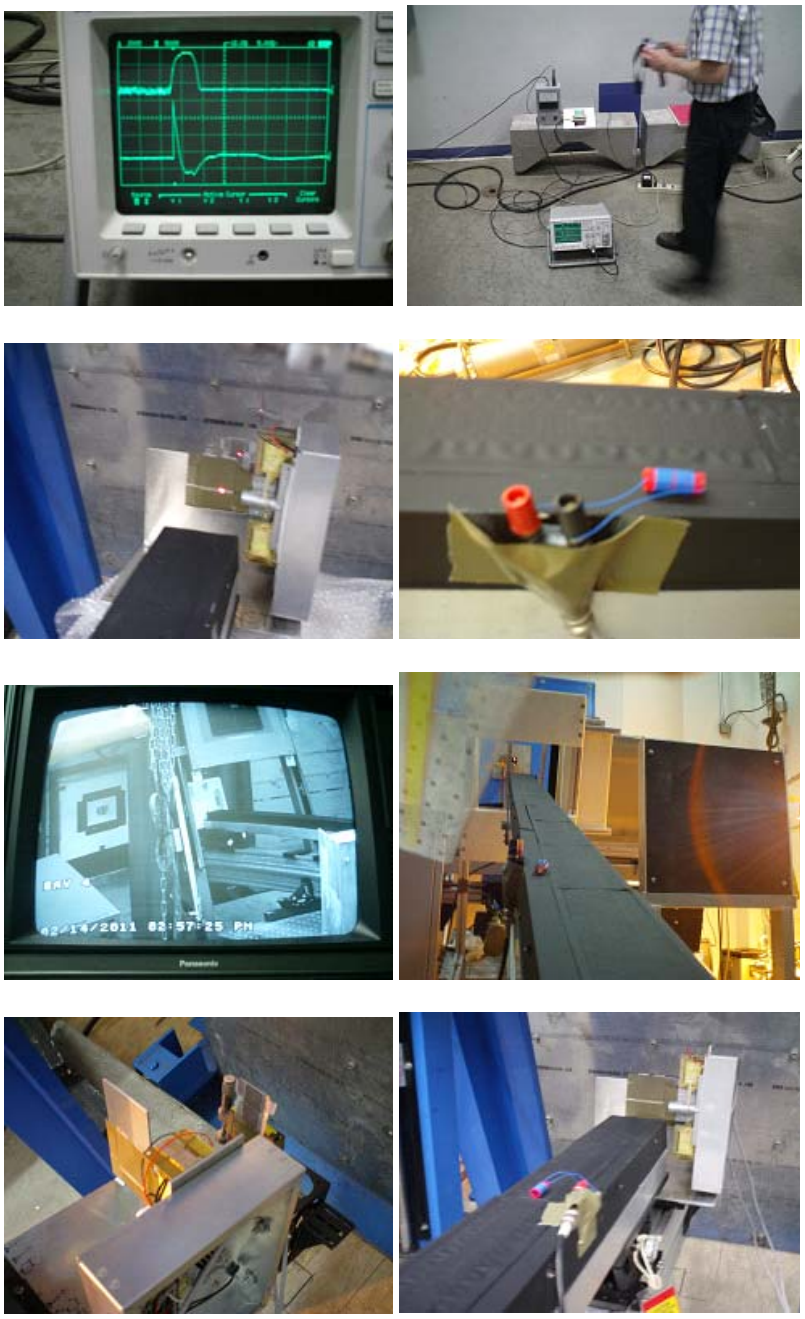

Fig. 15 The upper left photo is the pair of oscilloscope traces corresponding to the chopper. The top trace shows the slit 10 msec open time via a light beam that passes through the slit to a light detector whose output is the top trace. The bottom trace is the magnetic field pulse, which is measured by a small solenoid pick-up coil placed on the rail. The chopper slit is downstream of the second collimation slit at the PMF entrance.

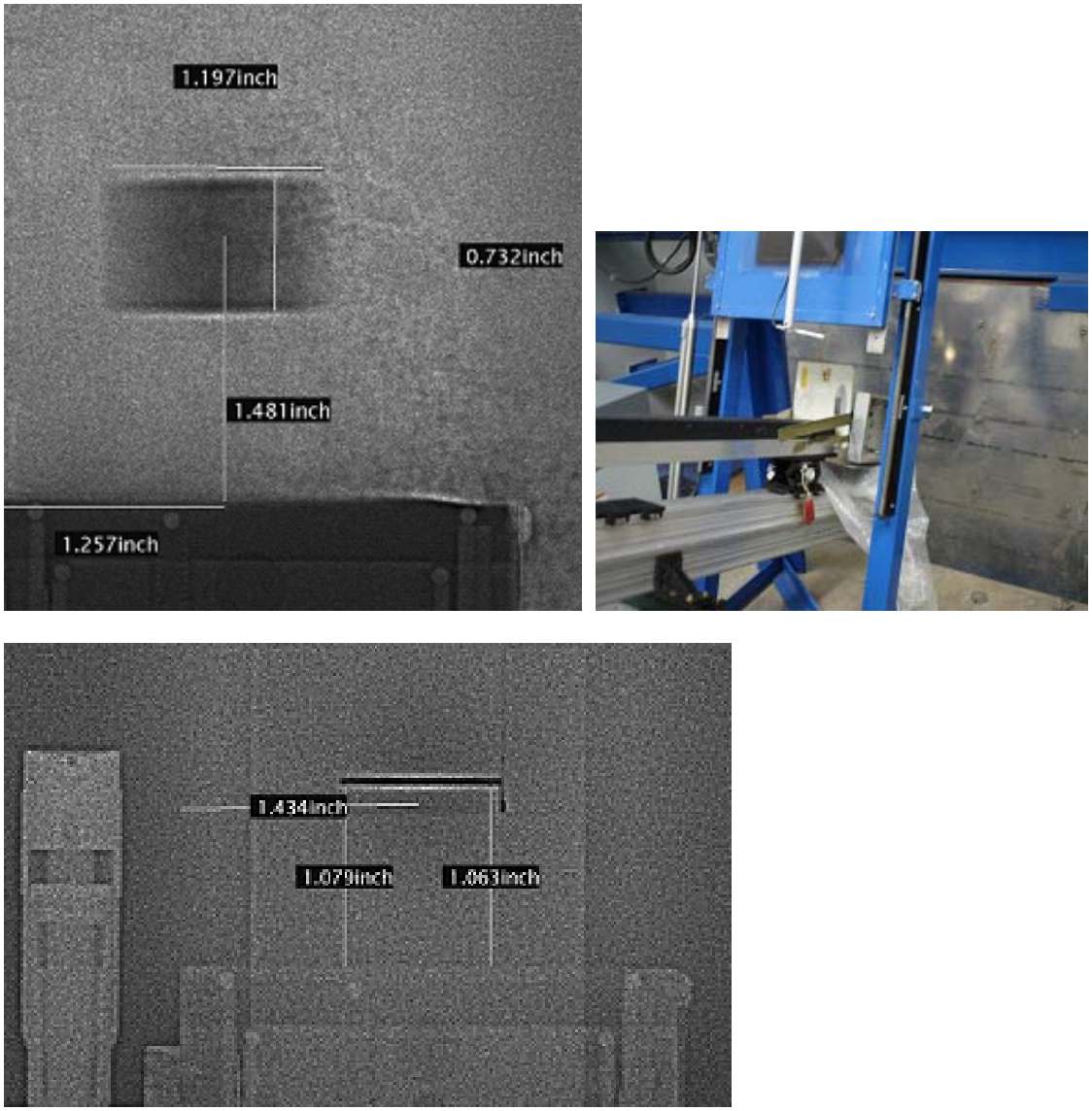

Fig. 16 (top) Shown is a neutron image of the first collimation slit taken with the Fuji film imaging plate (IP) set adjacent and in front (upstream) of the second collimation slit. (bottom) Shown is a neutron image taken with the IP placed adjacent but behind (downstream) of the second collimation slit. The second slit is set on the entrance of the PMF at the position of the fast shutter. The fast shutter is about 1 meter downstream of the massive shutter, and is used in the normal radiographic imaging of Bay 4. The fast shutter was left open for all experiments to allow placement of the PMF.

of the Bay 4 collimation tube and the chopper slit. In the normally closed position the chopper slit is above the second collimation slit by a few millimeters, which prevents the neutron beam from passing through the PMF to the Fuji film imaging plate.

The computer controlled chopper slit is coordinated with the computer controlled PMF pulsed power supply. When the computer commands the capacitors of the PMF power supply to charge, the chopper slit is in the normally closed position. And when the charging voltage of the

PMF capacitors in power supply is reached, the computer with appropriate delays triggers the chopper to move down past the level of the 2nd collimation slit. The chopper and slit is aligned with the 2nd collimation slit for approximately 10 msec. The timing is set so the 7.5 msec FWHM magnetic field pulse occurs when the two slits are aligned to allow passage of the neutron beam over the top of the PMF rail and onto the Fuji film detector. The chopper slit continues its passage downward and within a second is moving back up to its normally closed position. In the chopper slit upward movement, the two slits are again aligned to allow neutron beam passage over the PMF rail and onto the Fuji film plate when the magnetic field is off, and the capacitors of the PMF power supply are beginning to charge again for the next pulse.

In this manner the same Fuji film imaging plate can record the band of vertically deflected 1.8-3.0 Å spin-up neutrons, which are produced when the magnetic field pulses occur, and the band of un-deflected neutrons of all energies, which is produced when the magnetic field is off. Fig. 15 shows the small solenoid pickup coil to measure the pulsed magnetic field and align the magnetic field pulse with the pulse of the slit chopper and 2nd collimation slits, which allow transmission of the neutrons. The solenoid has a diameter of about 1 cm (the width of the north or south magnetic poles).

A small light emitting diode and light detector produce a pulse corresponding to the period of time when the chopper and 2nd collimation slits are sufficiently aligned. That is, the light can pass from the light emitting diode through the two slits to the light detector as long as the chopper and 2nd collimation slit have overlap. Thus, the timing the approximate 10 msec alignment of the chopper and 2nd collimation slit for maximum neutron transmission and the 7.5 msec FWHM magnetic field pulse could be coordinated. The magnetic field pulse from the solenoid coil varied significantly depending on placement, but was sufficiently reliable to indicate the onset of the magnetic field pulse.

The TV monitor photo in Fig. 15 shows the upstream collimation slit on the aluminum face plate, the chopper, and then the 2nd collimation slit at the PMF entrance. Another photo shows the chopper slit set to an open position in alignment with the second collimation slit, which then allows the laser light from the alignment laser at the bema stop to shine onto the massive concrete shutter door. The massive concrete shutter door blocks the view of the underlying aluminum faceplate with the attached first collimation slit.

In Fig. 16 (top) is a Fuji film image of the first collimation slit, which is set on the aluminum face plate of the Bay 4 collimation tube. The Fuji film plate is placed at the PMF entrance at the position where the second collimation slit is to be placed as shown in the photo at the bottom of Fig. 16. The second slit is then placed in its position at the PMF entrance and a Fuji film plate is put adjacent and downstream to image the alignment of the first and second collimation slits with the neutron beam. In Fig. 16 (middle) is the neutron image of the aligned 1st and 2nd collimation slits without the chopper.

The magnetic field of the PMF read a maximum of +/- 4.4 kilogauss at the surface of the PMF electric insulation, which was far lower than the expected 25 kilogauss level magnetic field. The PMF field serpentine winding were divided into 15 sections, each 20 cm and containing ten N-S periods. The manufacturer (Oersted) realized the sections had been wire in series instead of parallel. The series sections for an applied voltage produces much less magnetizing current than the 15 sections are wired in parallel. The same voltage applied to 15 sections in parallel was expected to produce much larger magnetizing currents.

The first set of PMF imaging experiments were conducted at the lower +/- 4.4 kilogauss surface magnetic field before shipping the PMF back to the manufacturer to reset the wiring to

parallel. The 15 serpentine winding sections of the PMF were re-wired to parallel by the manufacturer and shipped back to MNRC free of charge. However, the PMF surface magnetic field read only 50% more at +/- 6.1 kilogauss. The exponential decay of the magnetic field from the pole surfaces and the 1.5 mm distance gives an estimated +/- 7.8 kilogauss magnetic field at the pole surfaces, which is almost twice the magnetic field flux obtained with the permanent magnet PMF. However, the peak 0.78 T surface magnetic field was of the electromagnetic PMF

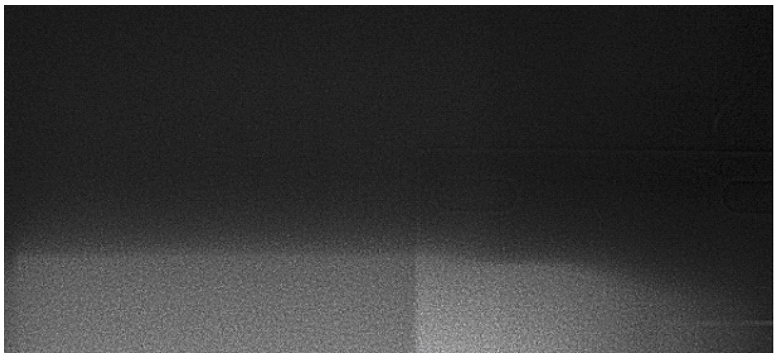

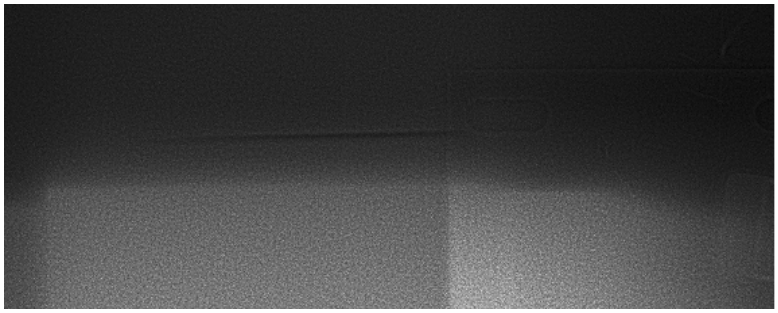

Fig. 17 Shown are two neutron images at maximal downstream position from PMF prior to chopper development. (top) Neutron image with reactor at 1 MW with 5400 sec (90 min) exposure time and Fuji imaging plate placed at maximal 7 meter downstream position from PMF entrance just in front of laser at beam stop as shown in bottom photo. The magnetizer pulsed current supply is set at 31 micro-farads and 700 volts to produce 11 msec FWHM magnetic field pulse duration in which 291 pulses were produced in the 90 min exposure time. (bottom) Longer magnetizing current pulse width is produced with higher 81 microfarad capacitance in which the magnetizer current supply is set at 700 volts to produce a 37 msec FWHM magnetic field pulse duration in which 133 pulses were produced in the 90 min exposure time. Again the neutron image was taken with reactor at 1 MW with 5400 second exposure time and Fuji imaging plate placed at maximal 7 meter downstream position from PMF entrance just in front of laser at beam stop.

about 4 times lower than the expected value.

Prior to the development of the chopper and the PMF re-wiring, the imaging experiments

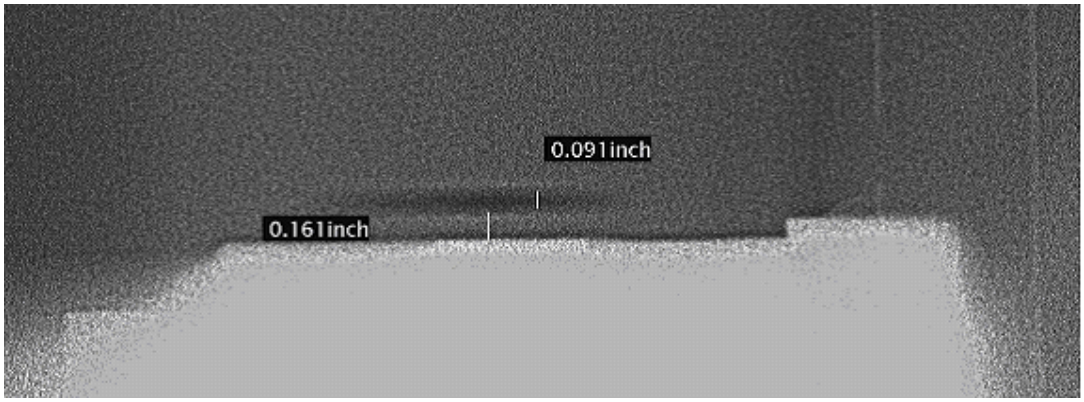

Fig 18 (a) Shot Number 1147-408. - Magnet off and chopper off, 1-hour exposure taken at downstream, beam-stop end of rail. As a result of lowering the rail alignment of the slit on face plate and the slit at the PMF entrance was completed.

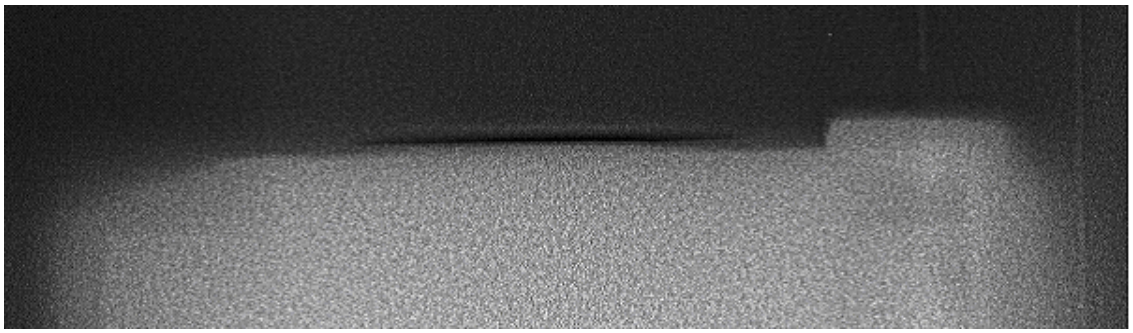

Fig. 18 (b) Shot Number 1146-417 Magnet on and chopper on, 1-hour exposure taken at the end of rail. The rail heating expanded the rail so the PMF surface rose about 0.200 inches or 5.0 mm, which began to eclipse the slit.

Fig 18 (c) Shown is a photo showing the placement of the Fuji imaging plate at the end of the PMF between the two rectangular borated polyethylene limiting apertures.

with the pulsed electromagnetic field PMF were performed. The charging and discharging of the PMF power supply to produce the magnetic field pulses were performed manually, and the number of magnetic field pulses was counted manually during the set neutron beam exposure time. We realized overheating would not be a problem with the windings in series. Hence, we were able to run at 700 volts and 80 mill-farad capacitance, which yielded 27 msec FWHM magnetic field pulses with a pulse repetition frequency of one pulse every 40 seconds.

The experimental results prior to the chopper, rewiring the PMF, and computer control are shown in Fig. 17. Shown are two neutron images at maximal downstream position from PMF prior to chopper development. The top neutron image in Fig. 17 was obtained with reactor at 1 MW power for a 5400 sec (90 min) exposure time. The Fuji imaging plate was placed at maximal 5.3 meter downstream position from the PMF entrance, which is just in front of laser at the beam stop as shown in the bottom photo. The top neutron image was obtained with the magnetizer pulsed current supply set at 30 micro-farads and 700 volts, which produced an 11 msec FWHM magnetic field pulse duration in which there were 291 magnetic field pulses in the 90 minute exposure time..

The bottom neutron image was taken with the magnetizing current pulse width set to a longer width of 27 msec FWHM, which was produced at 700 volts with the higher 81 microfarad capacitance setting in magnetizer current supply. This setting produced 133 magnetic field pulses in the 90 minute exposure time. Again the neutron image was obtained with reactor at 1 MW power for a 5400 second exposure time and Fuji imaging plate placed at maximal 5.3 meter downstream position from the PMF entrance just in front of laser at the beam stop.

The chopper was fabricated and the PMF was sent back to the manufacturer for re-wiring from series to parallel. With the chopper in place and the surface magnetic field of +/- 7800 kilogauss the imaging experiments with the electromagnetic PMF were conducted again. This time the computer controlled the PMF power supply charging and discharging of the capacitor banks to produced the magnetic field pulses of 11 msec FWHM, at a rate of 5.4 per minute with the capacitor bank set to 21 milli-farad. Oersted, the manufacturer recommended running PMF at no higher than 21 milli-farad at 700 volts as the PMF windings would overheat for higher capacitances (longer pulse lengths). The 21 milli-farad capacitance, 0.274 milli-henry inductance, and 0.439 ohm resistance set the magnetic field pulse width to 7.5 msec FWHM, and one magnetic field pulse could be produced about every 11 seconds.

We compared the results of the PMF magnetic field on and chopper on with the case of the magnetic field off and the chopper off, but set in the open position to allow the neutron beam to pass through the two collimations slits and over the surface of the rail to the Fuji film plate. The two collimation slits were set to send the neutron beam as close to the rail surface as possible, where there are the highest magnetic field vertical gradients. The magnetic field vertical gradient or change of magnetic field with distance above the PMF north and south magnetic pole surfaces produces the largest vertical deflection heights. The heating of the rail cause expansion. Hence, the slits were initially set to 0.161 inches or 4.0 mm above the rail insulation surface to allow heating expansion of the rail. After the heating expansion of the rail, we desired the bottom of the slit to be at 0.5 mm or slightly above the insulation surface of the rail.

The comparison of (1) the chopper turned off and adjusted to let the neutron beam pass over the rail at 4.0 mm height above the rail to a Fuji film imaging plate set at the end of the PMF rail, and (2) the PMF rail energized with magnetic field and the chopper operational, and the rail without magnetic field, and, is shown in Fig. 18 (b). With the chopper and magnetic field

off, we took a neutron image at the end of the cold PMF rail. The top neutron image in Fig. 18 (a) or Shot Number 1147-408 is with the magnetic field off and the chopper off and aligned to let the neutron beam pass over the PMF black insulation of the cold rail at a height of 4 mm for a 1 hour exposure. We then aligned the chopper and aligned the chopper with the two collimation slits and verified by the laser showing a glint of transmitted light and by a 30 minute neutron beam exposure. We then turned on the magnetic field of the rail and then calibrated the timing of the chopper slit with the PMF magnetic field pulses, which were controlled by a microprocessor.

Fig. 19 (a) Photo of the placement of the Fuji Film Imaging detector at the beam stop and alignment laser position, which is the maximum 5.3 meter distance downstream of the PMF entrance (with second collimation slit).

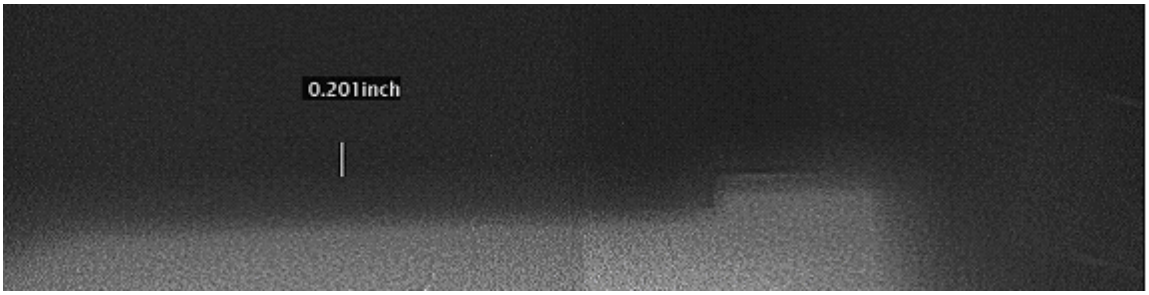

Fig. 19 (b) Shot Number 1147-409. - Magnet on and chopper on, 3.0-hour exposure taken at laser position at beam stop (shown in photo above). The horizontal band above the PMF rail surface is estimated to have a vertical width of about 0.2 inches (5 mm) and the bottom of the band is approximately 0.2 inch (5 mm) above the PMF surface. A diverging ray after the pair of collimation slits has vertical divergence angle $\theta_d = 6.7x10^{-4} rad$ at the PMF ray entrance, and the ray will attain a vertical height of 3.5 mm in the maximum 5.3 meter distance from the PMF entrance to the Fuji film plate imaging plate, which is placed at the Bay 4 beam stop next to the alignment laser. From

The rail was allowed to warm up for 30 minutes to allow for maximum thermal expansion. During the warm-up period the timing between the chopper slit and two collimation slits was adjusted and verified by the alignment of the oscilloscope traces of the shutter slit light beam indicator and magnetic field pulse. Also the peak magnetic field was measured and verified.

After the rail had reached thermal steady state, and the chopper and magnetic field pulses were verified to be in synchronism and in steady state operation, we took the next neutron image shot. The next neutron image shot was taken with the magnetic field on and the chopper on for a 1 hour exposure with the Fuji film plate again placed at the end of the PMF rail. The heating and expansion raised the rail 0.200 inches or 5.0 mm, which partly eclipsed the beam, as shown in Fig. 18 (b). This shot indicated the rail needed to be lowered slightly by 0.040 inches or 1.0 mm to leave a safe distance of 0.5 mm between the black surface insulation of the rail and the bottom of the pair of collimation slits in the neutron image. In Fig. 18 (c) or the bottom photo shows the placement of the Fuji imaging plate at the end of the PMF between the two rectangular borated polyethylene limiting apertures. Also, we confirmed clear neutron passage with the alignment laser.

Using the neutron images as a guide and confirmed by the laser we lowered the PMF rail by 0.040 inches (1.0 mm) to allow a safe 0.5 mm distance between the bottom horizontal line of the collimation slits and the surface line of the black insulation tape of the PMF rail. We then took a 3 hour exposure with the magnetic field on and the chopper on. Adjustment in time of the chopper slit light pulse with the magnetic field pulse was set, the PMF rail was run for 30 minutes to allow for maximum thermal expansion and steady state magnetic field pulsing and chopper slit operation. The Fuji film plate was then placed at the maximum 5.3 meter position at the beam stop next to the alignment laser as shown in the photo at the top Fig. 19 (a). In the bottom Fig. 19 (b) is the 3 hour neutron image at 5.3 meter from the PMF entrance.

The neutron image shows a horizontal band above the PMF rail surface, which is estimated to have a vertical width of about 0.2 inches (5 mm), and the bottom of the band is approximately 0.2 inch (5 mm) above the PMF surface. The center of the band is thus measured at 7.5 mm above the PMF pole surfaces.

A diverging ray after the pair of collimation slits has vertical divergence angle $\theta_d = 6.7x10^{-4} rad$ at the PMF ray entrance, and the ray will attain a vertical height of 3.5 mm in the maximum 5.3 meter distance from the PMF entrance to the Fuji film plate imaging plate, which is placed at the Bay 4 beam stop next to the alignment laser. The focal plane of the focused spin-up neutrons of all wavelengths is calculated to be approximately 4.2 mm above the PMF north-south pole surfaces, which assumes zero initial divergence angle. Consequently the calculated 4.2 mm focal plane height above the PMF poles and the calculated 3.5 mm vertical height due to the neutron beam divergence sums to a calculated 7.7 mm height expected for the focused spin-up neutrons of all wavelengths.

The measured 7.5 mm for the center of the band of neutrons above the PMF pole surfaces in the Fig. 19 (b) neutron image at the beam-stop position (5.3 meter from PMF entrance) is close to the calculated 7.7 mm focal plane height above the PMF pole surfaces for the spin-up neutrons. The non-focused neutrons spread and fill the image plane and reduce the contrast of the observed band of focused spin-up neutrons. The intensity of the non-focused neutrons is insufficient to form a definitive band of non-deflected, straight-through neutrons just above the PMF pole surfaces. Scatter of neutrons as well as gammas from the reactor fills the image plane reducing contrast. The focusing by the PMF is sufficient to produce a contrast band of deflected neutrons.

The deflected neutrons have been deflected by a time-varying, magnetic field amplitude, which has a peak of 0.78 T at the pole surface. The 0.78 T is inferred from the measured 0.61 T with the Hall probe placed tightly against the black insulation surface of the PMF. The magnetic field varies from 0 T to 0.78 T and back to 0 T in 50 msec with a full width half maximum (FWHM) of 7.5 msec. The variation of the magnetic field amplitude during the magnetic field pulse yields a time-varying, vertical, spatial magnetic field gradient. Each surface magnetic field and corresponding vertical gradient produces a corresponding focal plane for all neutron wavelengths. The axial focal distance of each neutron wavelength line focus, which is measured from the PMF entrance along the focal plane, increases with increasing neutron energy. That is, each amplitude and amplitude vertical gradient of the PMF magnetic field focuses neutrons of all wavelengths to a particular focal plane height above the PMF pole surface in which the focal plane height is dependent on the magnetic field amplitude and vertical gradient.

The time-varying vertical gradient of the magnetic field yields a time-varying deflection force, which yields a time-varying height of the focal plane for all neutron wavelengths range. Hence a single magnetic field pulse produces a range of focal plane heights in which at each particular magnetic field amplitude and vertical gradient there is one focal plane at a particular height above the PMF poles in which neutrons of all wavelengths focus. And on the focal plane, the neutrons of lower energy form a line focus closer to the PMF entrance and the higher energy neutrons from a line focus at a larger distance downstream of the PMF entrance.

In summary, the calculated 7.7 mm vertical height of the band of focused spin-up neutrons corresponded closely to the measured 7.5 mm height of the center line of the imaged band of neutrons. The band of deflected spin-up neutrons was 5 mm in vertical width and the bottom of the band was 5 mm above the surface of the PMF pole. The limited exposure time of 3 hours and the smaller 0.78 T magnetic field allowed focused and near focused neutrons of 1.8 Å to 2.6 Å neutrons, which were in the tails of the McClellan Nuclear Radiation Center Bay 4 Maxwell Boltzmann distribution of neutrons with peak flux at 1.1-1.2 Å. The electromagnetic PMF was expected to produce a 2.0 T peak magnetic field amplitude, which would be operational at a higher duty factor, rather than the as built 7.5 msec FWHM with pulse repetition frequency of 5.4 pulses per minute.

The fabricated pulsed electromagnetic PMF with chopper is expected to perform well on a cold, very cold or ultra cold beam line as a spectrometer or monochromator source of spin-up polarized neutron. In fact there may be a possible use of the PMF to do ultra-cold neutron trapping, see paper by A. I. Frank1, V. G. Nosov, Quantum Effects in a One-Dimensional Magnetic Gravitational Trap for Ultracold Neutrons, JETP Letters, Vol. 79, No. 7, 2004, pp. 313–315. The next step is to find a cold or very cold neutron facility, where further testing or use of the pulsed magnetic field PMF can be pursued.

Appendix

The magnetic array (figure 1) consists of a straight bar of 300 (equivalent full width) wound laminated teeth, in 15 sets laid end for end, each set having 20 teeth (that is, 19 full-width teeth and two end teeth of half width). The 20-tooth sets are made of stacks of insulated 20 gage (.91 mm) thick low-carbon steel laminations, 2.2 cm wide (direction normal to neutron travel, in the horizontal plane), each tooth 5.0 mm long (in the direction of neutron travel) with a following wound slot of 5.0 mm long for a half-period of 1 cm. The two end teeth of each section are one-half the width of the others, 2.5 mm. The active length of the entire array is 3.00 meters. The slots are each 14.3 mm deep. Windings in the slots between the teeth are in a zig-zag pattern. The windings have the equivalent of 5 turns per tooth of AWG Nr 12 wire. The wire has 2.05 mm bare diameter, double-insulated with an electrically insulating lacquer having a high temperature rating (200 deg C). The wound sections were “potted” in an electrical epoxy formulated for resistance to stress and shock. These sections were mounted on an aluminum beam with interconnecting windings, with three groups of five 20-tooth sections each, connected in parallel. The half-width teeth at each end of each section are in contact with the half-width teeth of the next section except for those at the extreme ends. There are therefore 150 spatial magnetic periods of 2 mm length each. The measured inductance (at low current) was 15 micro-henry, and the DC resistance was .020 ohms.

The current carried by the windings when in service depends on the voltage and capacitor settings of the pulse generator, both of which may be chosen by the operator. The voltage is infinitely adjustable, and the energy storage capacitance may be adjusted in 1.25 mF increments. The magnetic field strength is a function of the peak electrical current. The peak current may be

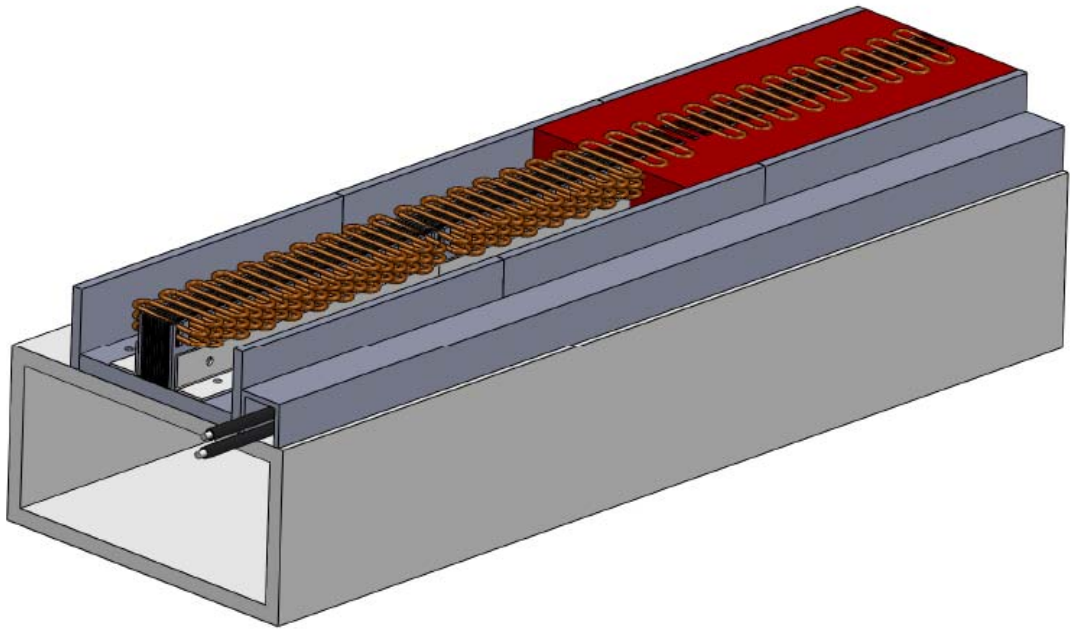

Fig. A1 Schematic of electromagnetic PMF designed and fabricated by Oersted Technology.

found by first writing the differential equation for the series combination of the voltages resulting from the circuit inductance L, capacitance C, and resistance R. For ease of application, the writer prefers a change of variables, using the resistance R plus the un-damped natural frequency ω_0 and the damping coefficient ρ,

$$\omega_0[hz] = \sqrt{\frac{1}{LC}} \tag{A1}$$

$$\rho = \frac{R}{2}\sqrt{\frac{C}{L}} \qquad \text{(dimensionless)} \tag{A2}$$

The solution breaks up into four cases, for $\rho < 1$, $\rho = 1$, $\rho > 1$, or for R = 0 (resulting in $\rho = 0$). The last case is physically unrealizable, but is nonetheless useful as a limit. The solution of the first case, $\rho < 1$, would result in an oscillatory response, but the pulse generator is designed to prevent reversal of current. The array was designed for this case, as it results in the highest peak current and thus field strength.

After solving for the current as a function of time, the result is differentiated with respect to time and set to zero to find the time at which peak current occurs. This is then substituted back into the solution to find the peak current. For the under-damped case, $\rho < 1$, the result is that the peak current i_{peak} is:

$$i_{peak} = k\frac{E_{ch\arg}}{R} \tag{A3}$$

$E_{ch\arg}$ denotes the initial charge voltage on the capacitors at the beginning of the pulse, where

$$k = 2\rho\exp(-U) \tag{A4}$$

$$U = \frac{\rho}{\sqrt{1-\rho^2}}\tan^{-1}\left(\frac{\sqrt{1-\rho^2}}{\rho}\right) \tag{A5}$$

The pulse generator has a source resistance at 20 mF setting of .017 ohms and inductance of 5 micro-Henrys.

The physical arrangement at the McClellan reactor and safety of the experimenters required long, low-resistance cables (2 each of 18.3 m AWG #2). These cables were added to the pulse generator, which resulted in an additional resistance of .019 ohms and inductance of 9.9 micro-henrys. The pulse generator was further modified for remote control from a hand-held console.

The total circuit resistance was therefore .056 ohms, and the circuit inductance was 29.9 ohms. Typical charging voltage was 725 Volts, and the capacitance setting was 21.25 mF. The calculated current in each circuit (1/3 the total), which based on this data, was 2837 ohms. The

current determined from interpolation of measurements was slightly higher (2900 amperes), however, which apparently was due to reduced inductance due to saturation at the peak current.

As the teeth are driven into and above magnetic saturation, the fields above them are not linearly proportional to current. At a peak current of 8700 amperes (2900 amperes in each set of 5 each with 20-tooth windings), the field just above the surface was .741 Tesla. The vertical field components versus altitude above the upper surface of the array at the center of the teeth are given in Table 1 below.

Table 1 Magnetic Field vs. Vertical Height Above PMF Magnet Surface

Vertical Distance above PMF surface (mm)	Magnetic field (Tesla)
0.076	0.741
1.0	0.672
2.0	0.539
3.0	0.408
4.0	0.301
5.0	0.221

Figure 2 shows a finite-element model of the magnetic fields of the toothed structure, and also the model arrangement. Figure 3 is a plot of the field normal to a line drawn between two points (visible in the model) at 1 cm above the surface. Figure 4 shows the field versus height tangential to a line drawn vertically through the center of a tooth. Figure 5 shows the electromagnetic PMF being tested at the Oersted facility in Troutdale, Oregon.

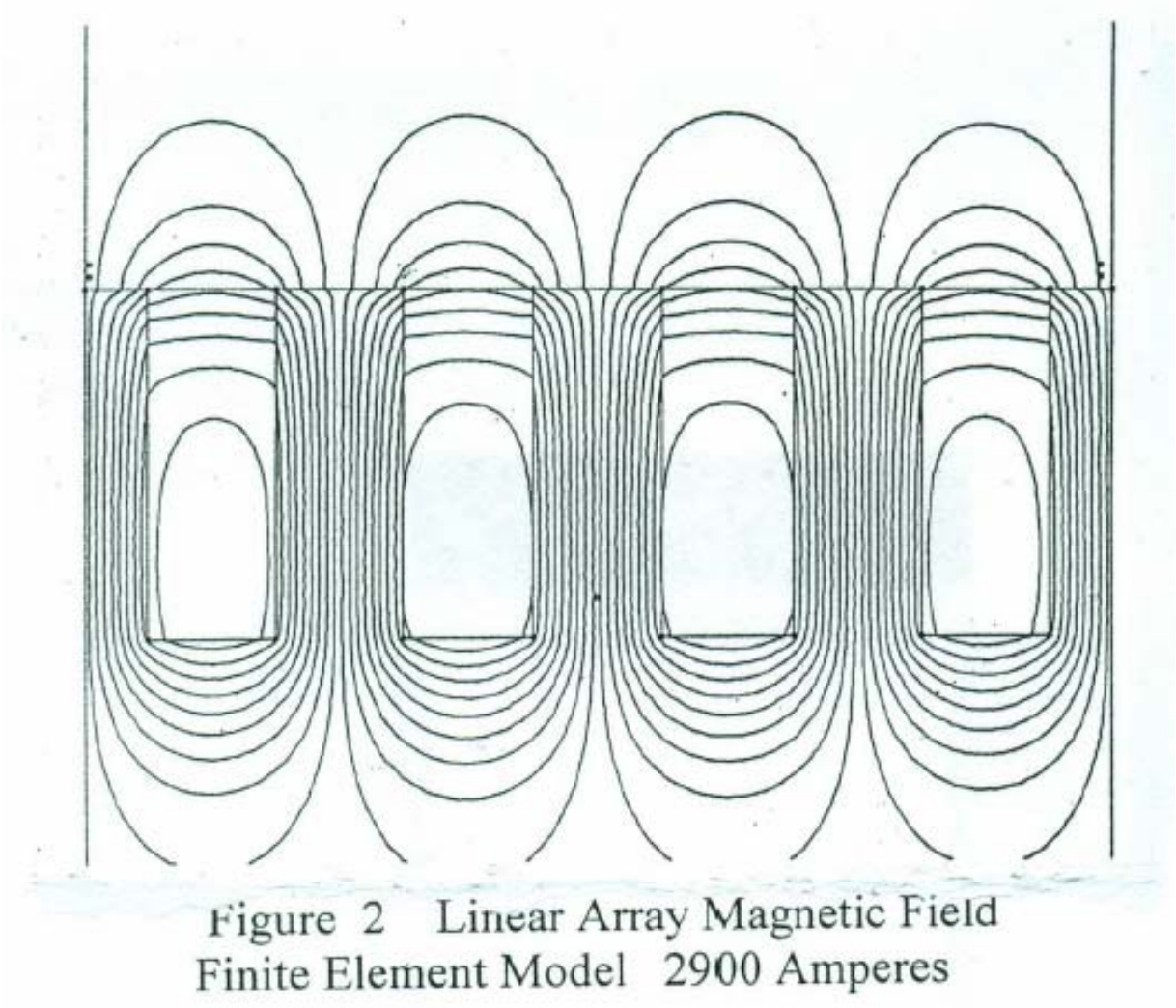

Fig. A2 Oersted Technology finite element calculation of PMF magnetic field is plotted. Shown is finite-element model of the magnetic fields of the toothed structure, and also the model arrangement.

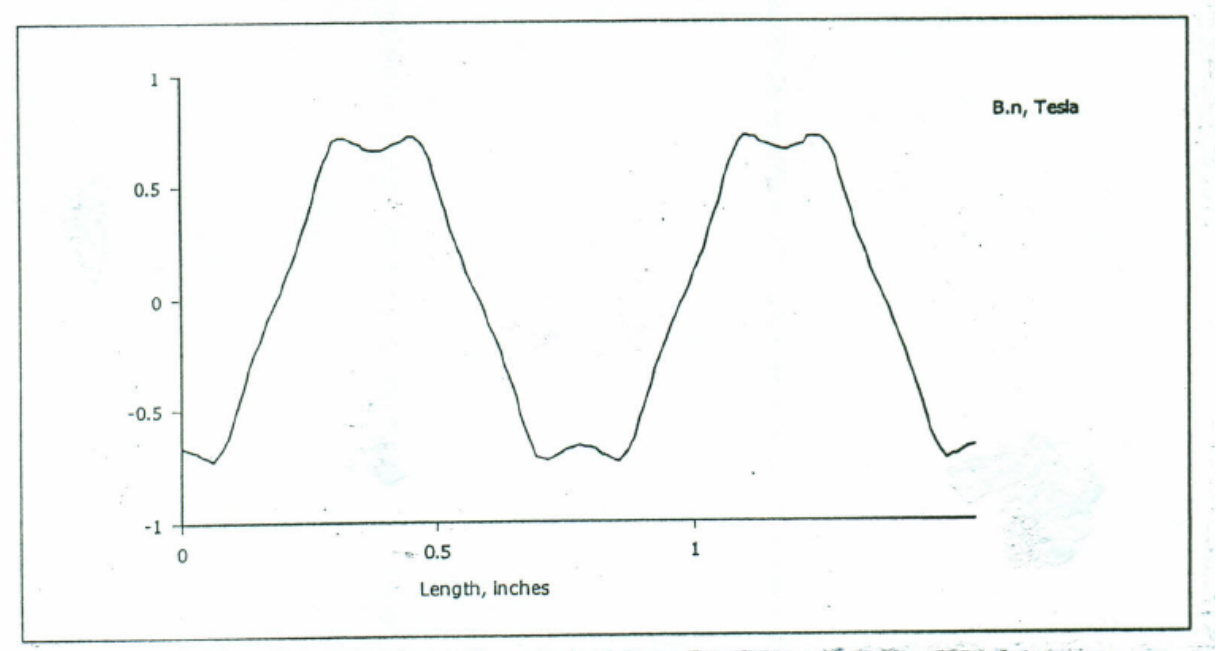

Figure 3 Vertical Component of Magnetic Flux Density B_y Along a Horizontal Line1 cm Above the Array on Centerline.

Fig. A3 Oersted Technology finite element calculation of PMF vertical magnetic field component - shown is plot of the field normal to a line drawn between two points (visible in the model) at 1 cm above the surface.

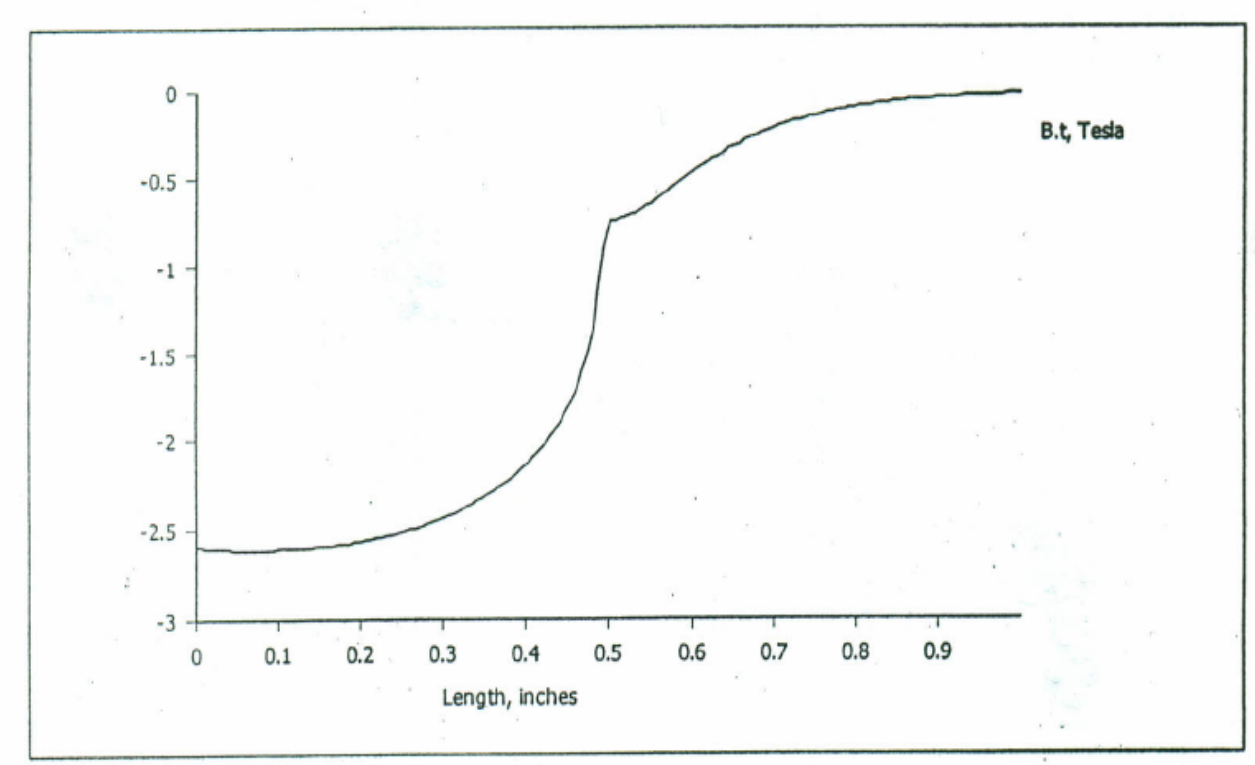

Figure 4 Vertical Component of Flux Density By Along a Vertical Line at a Tooth Center

Fig. A4 Oersted Technology finite element calculation of PMF - plotted is the magnetic field versus height tangential to a line drawn vertically through the center of a tooth.

Fig. A5 Photo of electromagnetic PMF being tested at the Oersted facility in Troutdale, Oregon.